ISSN 2075-1133, Inorganic Materials: Applied Research, 2020, Vol. 11, No. 5, pp. 1165–1172. © Pleiades Publishing, Ltd., 2020.
Russian Text © The Author(s), 2020, published in Perspektivnye Materialy, 2020, No. 1, pp. 33–42.

GENERAL-PURPOSE MATERIALS

Structure and Properties of $Ti_{28}Ni_{50}Hf_{22}$ Powder Alloy

S. S. Volodko[a], *, S. N. Yudin[b], **, V. V. Cheverikin[c], *, A. V. Kasimtsev[b], ****, G. V. Markova[a], *****, T. A. Sviridova[c], ******, B. V. Karpov[d], *******, S. S. Goncharov[a], ********, and I. A. Alimov[a], *********

[a] *Tula State University, Tula, 3000120 Russia*

[b] *OOO Metsintez, Tula, 300041 Russia*

[c] *National University of Science and Technology MISiS, Moscow, 119049 Russia*

[d] *Research and Development Center, Center for Pressure Metal Treatment on the Base of National University of Science and Technology MISiS, Moscow, Russia*

**e-mail: volodko.sv@yandex.ru*

***e-mail: sergey-usn@mail.ru*

****e-mail: cheverikin80@rambler.ru*

*****e-mail: metsintez@yandex.ru*

******e-mail: ya.gal-markova2012@yandex.ru*

*******e-mail: tim-17@yandex.ru*

********e-mail: omd.misis@mail.ru*

*********e-mail: gss160154@yandex.ru*

**********e-mail: alimov.iwann@mail.ru*

Received June 14, 2019; revised July 16, 2019; accepted July 19, 2019

Abstract—The effect of consolidation and thermal treatment on the structure, local chemical composition, and martensite transformation temperatures of the $Ti_{28}Ni_{50}Hf_{22}$ powder alloy is studied. It is shown that, in the powder state, the alloy is characterized by an inhomogeneous distribution of Ti and Hf in the matrix, whose concentration spread may reach 27 at %. Vacuum sintering and homogenizing annealing lead to equalization of the chemical composition. During powder sintering, the spread of Ti and Hf concentrations reduces from 27 to 2 at %. Subsequent vacuum annealing at a temperature of 1000°C for 4 h for a sintered sample additionally reduces the spread of concentrations from 4 to 2 at %, while the increase in the annealing duration from 4 to 16 h does not affect the uniformity of the element distribution. It is established that, at a large inhomogeneity of the chemical composition, the differential scanning calorimetry (DSC) methods fail to record the occurrence of martensitic transformation in the melt. However, homogenization of the alloy leads to the appearance of endothermic peaks on the DSC curve upon heating, as well as to narrowing of the interval of reverse martensitic transformation.

Keywords: calcium hydride synthesis, alloy with a high temperature shape memory effect, martensitic transformation, powder metallurgy, consolidation, thermal treatment, structure

DOI: 10.1134/S2075113320050354

INTRODUCTION

Shape memory alloys (SMAs) have been widely used in different areas of human activity owing to unique properties, such as a shape memory effect (SME) and superelasticity (SE). Currently, the development of nuclear power and the aerospace industry [1, 2] requires the use of alloys with a high-temperature shape memory effect in which the temperature interval of implementing the SME is above 100°C, typical of binary TiNi alloys that undergo thermoelastic martensitic transformation (TMT). Alloying of TiNi intermetallic with such elements as Hf or Zr is an effective method to increase the TMT of TiNi alloy to 300–500°C [1, 3]. Obtaining such three- and four-component alloys of the Ti–Ni–Hf/Zr systems by vacuum-arc and vacuum-induction melting is significantly complicated by the difference in the melting temperatures and densities of the alloy components, which leads to the development of liquation during crystallization, which is removed by 5–6 remelts of an ingot and long-term homogenizing annealing. For this reason, some studies use alternative methods of obtaining bulk polycrystalline SMAs based on the Ti–Ni–Hf and Ti–Ni–Hf–Zr systems [4–9]. However, at this moment, the problem of making homogenous compact ingots from a TiNi intermetallic alloyed by

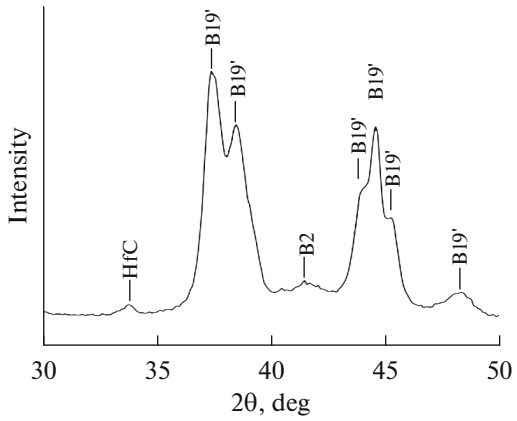

Fig. 1. Fragment of the powder diffraction spectrum.

refractory and heavy elements has not been solved completely [2, 10].

There is a similar problem for the binary TiNi alloys [11]. It is shown in [12, 13] that the binary TiNi alloys homogeneous in composition and having a high level of SME and mechanical properties are produced by the method of calcium hydride synthesis and the subsequent consolidation under the experimental conditions.

Calcium hydride synthesis refers to the metal-thermal method by which an alloy is obtained in reduction of metals from their compounds (oxides, chlorides) using calcium hydride to pure metals and their further interaction in molten calcium. This method was described in detail in [14]. At present, studies have been performed to obtain alloy powders of the Ti–Ni–Hf/Zr systems by the method of calcium hydride synthesis [15]; however, a consolidated state has not been examined.

The purpose of this work is to evaluate the effect of different parameters of consolidation and subsequent thermal treatment on the microstructure and homogeneity of chemical composition and MT temperature of the $Ti_{28}Ni_{50}Hf_{22}$ alloy produced from calcium hydride powders.

MATERIALS AND METHODS

The object of investigation was a pilot lot of $Ti_{28}Ni_{50}Hf_{22}$ alloy powder that was produced by the calcium hydride synthesis technology. The procedure for the powder production was described in detail in [15].

The powder compaction was performed using a CIP 62330 cold hydrostatic press (Avure Technologies, USA) with a working pressure of 200 MPa and holding for 3 min. Sintering and annealing were carried in an ESKVE-1/16GM12 vacuum chamber electric furnace in a vacuum of 5×10^{-5} mm Hg (6.66×10^{-3} Pa). The porosity was determined by the metallographic method using an AxioObserver D1m optical microscope (Carl Zeiss).

The phase composition of the samples was studied with a DRON-3 automated diffractometer using monochromatic CuK_α radiation with wavelength λ = 1.54178 Å.

The microstructural and local chemical analyses were performed by the method of scanning electron microscopy (SEM) using a TESCAN VEGA LMH scanning electron microscope with an attachment for elemental analysis of sample microvolumes.

The total chemical composition of the alloy was determined by the method of inductively coupled plasma atomic emission spectrometry and the method of X-ray fluorescence spectroscopy. The error of estimating the content of the main elements was ±2%. The content of gas-forming impurities was analyzed using Leco equipment (USA): a TC-600 oxygen and nitrogen analyzer, a CS-400 carbon analyzer, and a RHEN-602 hydrogen analyzer.

The melting temperature and the temperatures of martensite transformations of the alloy were studied using differential scanning calorimetry (a SETARAM calorimeter in an argon current of 60 mL/min at a heating rate of 10°C/min).

RESULTS AND DISCUSSION

Figure 1 presents the diffraction spectrum and the phase composition of the powder. The phase analysis showed that, at room temperature, the melt structure consists primarily of B19' martensite with an *mP*4/2 monoclinic lattice and parameters $a' = 0.3084$, $b' = 0.4068$, $c' = 0.4921$ nm and angle $\beta = 103.792°$. There are reflections corresponding to B2-austenite with a *cP*2/1 cubic lattice and trace amounts of hafnium carbide.

Table 1 shows the chemical powder composition which is close to the stoichiometric composition. The high content of hydrogen in the powder is a peculiarity

Table 1. Chemical composition of the $Ti_{28}Ni_{50}Hf_{22}$ powder (Ti–35.8 N–47.9 Hf)

Alloy composition at % (wt %)							
Main elements, at % (wt %)			Impurities, wt %				
Ni	Ti	Hf	O	N	C	H	Ca
49.9 (35.5)	28.4 (16.5)	21.7 (46.8)	0.093	0.036	0.040	0.300	0.090

of the technology. After vacuum annealing of the powder at 800°C for 30 min, the hydrogen level decreased to 0.004 wt %.

Figure 2 demonstrates the SEM image for the surface of the microsection of the $Ti_{28}Ni_{50}Hf_{22}$ alloy powder particles obtained in the mode of recording the backscattered electrons. The local X-ray microanalysis of separate particles (Table 2) showed nonuniform distribution of the components in the alloy between the particles.

Ni is distributed through the structure most uniformly; the spread of its concentration does not exceed 1.6 at %. For Hf and Ti, the concentration spread may reach 27 at % in the extreme case. However, the distribution of the components within one powder particle is rather homogeneous, which may be seen in spectra *6*, *7*, and *13*, *14* (Fig. 2, Table 2).

At present, we know that, during the calcium hydride synthesis, alloy formation occurs by diffusion of a highly soluble component in calcium to the particles of the component that is poorly soluble in liquid calcium. Thus, the alloy homogeneity during the calcium hydride synthesis is determined by solubility and diffusive mobility of the components in liquid calcium. For the case of a ternary Ti–Ni–Hf system, where the Ti and Hf solubility in molten calcium does not exceed hundredths of a percent [16], their uniform distribution in the alloy depends strongly on homogeneity of mixing the raw components and the size of initial TiO_2 and HfO_2. Hence, the chemical composition of a separate particle will be determined to a great extent by the quantity of titanium oxide and hafnium particles that make contact with each other. A relatively uniform distribution of Ni in the entire powder volume is explained by its high solubility in liquid calcium (~81 wt % at 1200°C) [16]; therefore, it freely diffuses through the liquid phase to the Ti and Hf particles and interacts with them diffusively.

To study the structure and homogeneity of distribution of the powder alloy components in a compact state, the powder was compacted by uniform isostatic pressing and then was sintered in a vacuum at T = 1250°C for 2 h. The sintering temperature was selected on the basis of the temperature of melting of loose powder T_m = 1281°C calculated by the DSC method.

Figure 3 illustrates the structure of the alloy after sintering. It shows that nonuniformity of the chemical composition (Table 3), which is inherent to the powder, remained in the sintered sample. Figure 3a shows that Ni is distributed homogeneously within three expowder particles (grains). The difference in the Ti and Hf contents decreased significantly in grains compared to the powder state; however, it remained appreciable. Table 3 presents the results of micro-X-ray spectral analysis in the different regions of the microsection of the alloy in a compact state (X-ray microanalysis spectra are displayed in Fig. 3b). The Hf and Ti contents may vary within 12 at % with respect to the

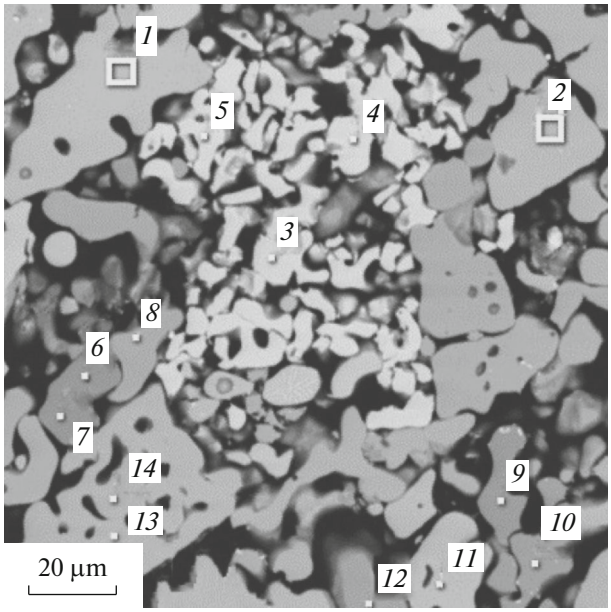

Fig. 2. Microstructure of the $Ti_{28}Ni_{50}Hf_{22}$ powder.

place of scanning. The structure has bright dispersed precipitates, in which the Hf concentration varies from 60 to 75 at %. Such inclusions of similar morphology were found in [17, 18]. In [17], such precipitates were identified as HfC. It was reported in [18]

Table 2. Results of X-ray spectral analysis of the powder

Spectrum no.	Main elements, at %		
	Ti	Ni	Hf
1	24.96	49.33	25.71
2	26.85	49.45	23.70
3	13.06	49.49	37.45
4	13.05	50.28	36.67
5	12.69	49.08	38.23
6	38.95	49.04	12.01
7	39.25	48.9	11.85
8	32.32	49.25	18.43
9	36.42	49.99	13.59
10	35.47	49.68	14.85
11	25.16	48.96	25.88
12	33.56	50.47	15.97
13	28.33	49.15	22.52
14	28.17	49.17	22.66

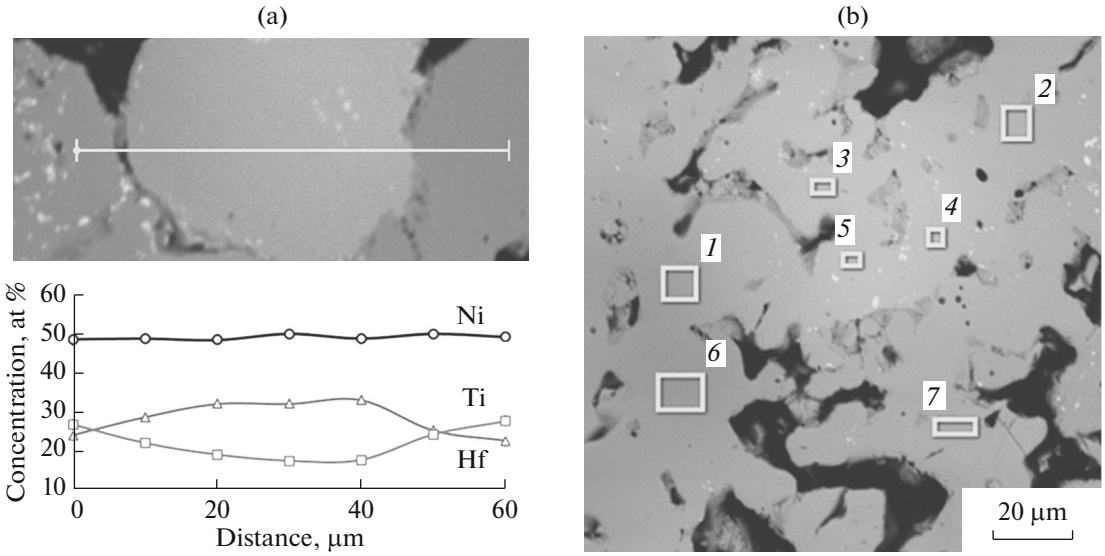

Fig. 3a. (a) Distribution of elements along several grains; (b) the region of determination of the local elemental composition of the alloy, after sintering at 1250°C for 2 h.

that as a rule HfO_2 is formed in alloys rich in Hf and/or Ni alloys. On the basis of X-ray studies (Fig. 1), we may assume that the bright inclusions in the alloy examined represent either hafnium carbide or hafnium oxycarbide.

In addition, we note a rather high open and closed porosity of the sintered sample, which according to the data of metallographic studies is found at the level of 40%. At such high porosity, the contact area of the particles is small, and the diffusive redistribution of such components as Hf and Ti will hardly be possible in the sample volume; therefore, it was decided not to perform further homogeneous annealing on this sample.

The high porosity value in sintering of the $Ti_{28}Ni_{50}Hf_{22}$ alloy powder is evidently related to low diffusive mobility of Hf in the TiNi lattice, as well as to reduced melting temperatures of the powders and, consequently, a nonoptimal sintering temperature. The difference of T_m of disperse particles from bulk materials may be caused by several factors, e.g., adsorbed gases, dispersiveness of powder, etc. After sintering the alloy at 1250°C for 2 h, its melting temperature was already T_m = 1310°C.

Figure 4 shows the structure of the sample after vacuum sintering at 1300°C and holding for 3 h. According to the data of the metallographic study, the porosity decreased to 10% compared to the previous sintering and became completely closed. The spread of Hf and Ti concentrations calculated in three different visual fields was 4 at % on average, which is significantly smaller than in the sample after sintering in the mode at 1250°C for 2 h. The difference in the Ni content is ~1 at %. In general, we note a positive effect of the increased sintering temperature and the increased isothermal holding time on the homogeneous distribution of the components in the sintered alloy sample.

To achieve more uniform distribution of the components through the volume, homogenization annealing of the samples was performed. Figures 5a and 5b present the microstructures of the alloy samples that were sintered at 1000°C for 4 and 16 h; Table 5 illustrates the results of the local chemical analysis. The

Table 3. Results of X-ray spectral analysis of the alloys

Spectrum no.	Main elements, at %		
	Ti	Ni	Hf
1	34	49.2	16.8
2	27	49.5	23.5
3	23	49.3	27.7
4	23	49.1	27.9
5	23	49.4	27.6
6	35	49.2	15.8
7	29	49.5	21.5

Table 4. Results of X-ray spectral analysis to Fig. 4

Spectrum no.	Main elements, at %		
	Ti	Ni	Hf
1	27.83	49.09	23.08
2	28.19	49.06	22.75
3	27.99	49.51	22.5
4	29.93	49.08	20.99
5	31.03	49.65	19.32

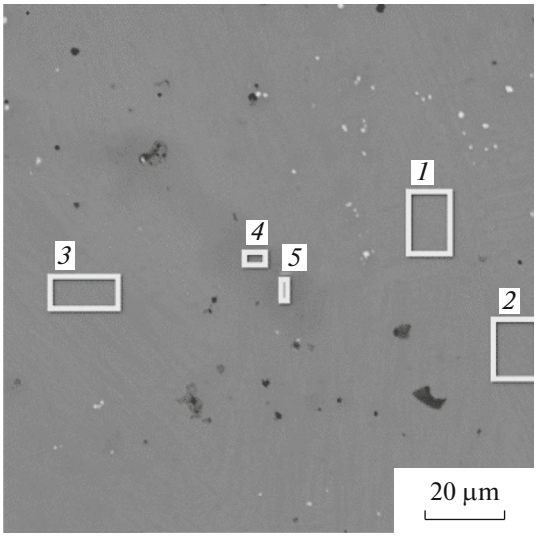

Fig. 4. Microstructure of the alloy after sintering at 1300°C for 3 h.

spread of Ni concentrations after annealing for 4 and 16 h was the same and amounted to about 1–1.2 at % with respect to the place of scanning, which is similar to the sample sintered at 1300°C for 3 h. The determination of the local chemical composition in three different visual fields showed that the spread of Hf and Ti concentrations in the sample after annealing at 1000°C for 4 h decreased from 4 to 2 at % compared to the sintered state. Annealing for 16 h did not affect much the distribution of Hf and Ti in the sample. Thus, we may assume that the further annealing for longer than 16 h is impractical, and a more homogenous alloy can be obtained only by optimizing the technological parameters of the calcium hydride synthesis.

An important characteristic of SMA is the MT temperature intervals. To monitor the effect of the parameters of sintering and thermal treatment on the MT temperatures, studies were carried using a differential scanning calorimeter in the mode of heating to 400°C. The results are depicted in Fig. 6. The endothermic peaks recorded made it possible to determine the temperatures of the start (A_s) and the finish (A_f) of the reverse MT and the other characteristics from Table 6.

Upon heating the sintered sample in the mode of 1250°C for 2 h, no effects were recorded on the DSC curve. The absence of a peak can be explained by the sensitivity of temperatures of the B19' ↔ B2 transition to the concentration of elements in the alloy. A set of solid solutions with different concentration of Hf and Ti (Fig. 3, Table 3) favors the development of reverse martensite transformation in a very wide temperature interval, and consequently, the peak is spread across the whole temperature interval of study; a similar effect was observed in [12]. Sintering in the mode of

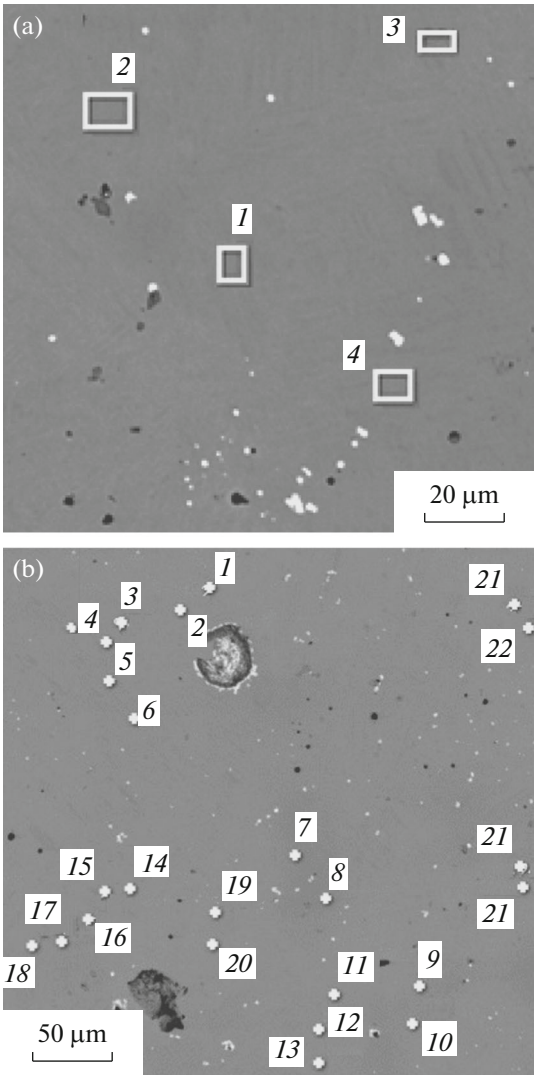

Fig. 5. Structure of the sample after vacuum sintering at 1300°C for 3 h and annealing at 1000°C for (a) 4 and (b) 16 h.

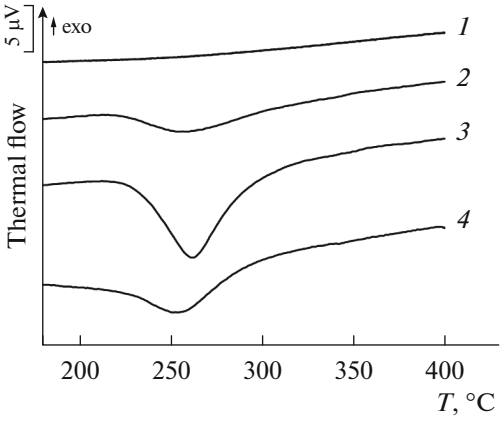

Fig. 6. DSC curves obtained by heating the alloys in different modes: (*1*) sintering at 1250°C for 2 h; (*2*) sintering at 1300°C for 3 h; (*3*) sintering at 1300°C for 3 h + annealing at 1000°C for 4 h; (*4*) sintering at 1300°C for 3 h + annealing at 1000°C for 16 h.

Table 5. Results of X-ray spectral analysis to Fig. 5

Spectrum no.	Main elements, at %		
	Ti	Ni	Hf
Annealing at 1000°C for 4 h			
1	29.3	49.78	20.92
2	28.78	49.12	22.1
3	29.08	49	21.92
4	28.69	48.6	22.71
Annealing at 1000°C for 16 h			
1	29.35	49.34	21.31
2	29.13	48.86	22.01
3	29.46	48.72	21.81
4	29.26	49.37	21.37
5	29	49.25	21.76
6	28.88	49.35	21.77
7	30.61	49.1	20.3
8	30.58	48.89	20.53
9	29.85	49.04	21.11
10	29.73	49.3	20.97
11	29.17	48.77	22.06
12	29.18	48.91	21.9
13	29.17	49.18	21.65
14	28.98	49.26	21.75
15	29.32	49.32	21.37
16	29.29	49.4	21.31
17	29.74	48.97	21.28
18	28.89	49.42	21.69
19	28.89	49.72	21.39
20	28.78	49.43	21.79
21	29.27	49.15	21.58
22	29.32	49.05	21.63
23	29.13	49.44	21.43
24	29.06	49.63	21.32

Table 6. Characteristics of martensitic transformations of the alloy upon heating

State	A_s, °C	A_f, °C	$A_f - A_s$, °C
Sintering at 1300°C, for 3 h	221	306	85
Sintering at 1300°C for 3 h + annealing at 1000°C for 4 h	231	294	63
Sintering at 1300°C for 3 h + annealing at 1000°C for 16 h	227	291	64

1300°C for 3 h provides a more uniform distribution of elements in the alloy (Fig. 4, Table 4); therefore, a small peak is recorded on the DSC curve. The subsequent annealing at 1000°C for 4 and 16 h leads to the appearance of more pronounced peaks. This evidently happens because of equalization of the chemical composition, especially concerning the Ti and Hf concentrations. The homogenization during annealing leads to a decrease in the $A_f - A_s$ value, i.e., the shortening of the interval for reverse MT. At an increase in the

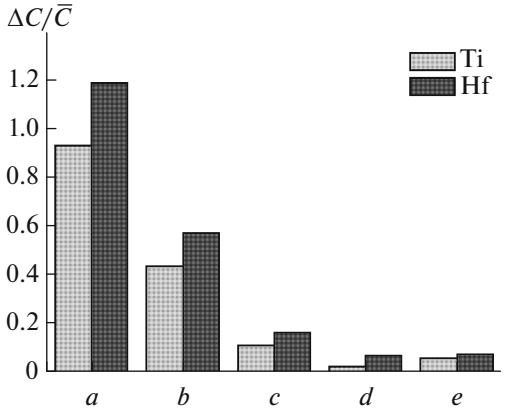

Fig. 7. Homogeneity of alloy depending on the technological stage: (*a*) powder; (*b*) sintering at 1250°C for 2 h; (*c*) sintering at 1300°C for 3 h; (*d*) sintering at 1300°C for 3 h + annealing at 1000°C for 4 h; (*e*) sintering at 1300°C for 3 h + annealing at 1000°C for 16 h.

annealing time to 16 h, the A_f and A_s temperatures shift slightly to the region of lower temperatures, and the peak becomes flatter, which is likely related to the change in the composition of the matrix during dissolving/precipitation of secondary phases upon annealing, e.g., Hf-rich phases.

This work demonstrates that, during the transition from one technological operation to another (alloy powder synthesis → vacuum sintering at 1250 or 1300°C → vacuum annealing of the sintered samples at 1000°C over different time), the alloy homogeneity constantly increases. This is demonstrated in Fig. 7. The ratio of the Ti and Hf concentration spread ($\Delta C = C_{max} - C_{min}$) in the matrix to the average concentration of the elements ($\bar{C}$) in the alloy was used as the criterion of homogeneity.

It is seen from Fig. 7 that the powder state is characterized by inhomogeneous spread of Ti and Hf (Fig. 7a). The consolidation considerably increases the alloy homogeneity; it is the stronger, the higher the sintering temperature (Figs. 7b, 7c); and the homogenizing annealing cycles make it possible to additionally improve uniformity of distribution of the components in the matrix.

CONCLUSIONS

1. The structure of the synthesized calcium hydride powder of $Ti_{28}Ni_{50}Hf_{22}$ alloy was represented primarily by B19' martensite. However, the micro-X-ray spectral analysis showed that the distribution of the components, especially Hf and Ti, was nonuniform in the powder.

2. During vacuum sintering of the powder, the distribution of the components in the alloy became more homogeneous. In the sintered sample, in the mode at 1250°C (0.95 T_m) for 2 h, nonuniform distribution of the components remained, the spread of Ti and Hf concentrations was 12 at %, and the porosity was at the level of 40%. After sintering at a temperature of 1300°C (0.99 T_m) for 3 h, the spread of Ti and Hf concentrations in the alloy decreased to 4 at %, and the porosity value dropped to 10%.

3. Isothermal annealing of the sintered alloy at 1000°C led to equalization of the chemical composition. The spread of Hf and Ti concentrations in the alloy decreased from 4 to 2 at %. The increase in the annealing time from 4 to 16 h did not significantly affect the uniformity of distribution of the components.

4. It was shown that the alloy homogeneity noticeably affected the occurrence of martensite transformation. No effects related to MT were found in the sample with the highest inhomogeneity of the chemical composition upon heating. As the alloy homogeneity increased during the thermal treatments, endothermic peaks were recorded on the DSC curve and the MT interval narrowed, while the temperatures of the reverse martensite transformation slightly decreased.

ACKNOWLEDGMENTS

This work was supported by the Russian Foundation for Basic Research (project no. 18-03-00451 A).

REFERENCES

1. Ma, J., Karaman, I., and Noebe, R.D., High temperature shape memory alloys, *Int. Mater. Rev.*, 2010, vol. 55, pp. 257–315.
2. Popov, N.N., Presnyakov, D.V., Morozova, T.A., and Grishin, E.N., Study of the structure and properties of high-temperature shape-memory alloys of the Ti–Pd–Ni and Ni–Ti–Hf systems, *Inorg. Mater.: Appl. Res.*, 2019, vol. 10, no. 4, pp. 853–864.
3. Karaca, H.E., Acar, E., Tobe, H., and Saghaian, S.M., NiTiHf-based shape memory alloys, *Mater. Sci. Technol.*, 2014, vol. 30, pp. 1530–1544.
4. Wang, B.X., Bhagat, R., Lan, X.Z., and Dashwood, R.J., Production of Ni–35Ti–15Hf alloy via the FFC Cambridge process, *J. Electrochem. Soc.*, 2011, vol. 158, pp. 595–602.
5. Yi, X., Meng, X., Cai, W., and Zhao, L., Multi-stage martensitic transformation behaviors and microstructural characteristics of Ti–Ni–Hf high temperature shape memory alloy powders, *J. Alloys Compd.*, 2019, vol. 781, pp. 644–656.
6. Elahinia, M., Moghaddam, N.S., Amerinatanzi, A., Saedi, S., Toker, G.P., Karaca, H., Bigelow, G.S., and Benafam, O., Additive manufacturing of NiTiHf high temperature shape memory alloy, *Scr. Mater.*, 2018, vol. 145, pp. 90–94.
7. Moshref-Javadi, M., Belbasi, M., Hossein Seyedein, S., and Taghi Salehi, M., Fabrication of (Ti,Hf)-rich NiTiHf alloy using graphitic mold and crucible, *J. Mater. Sci. Technol.*, 2014, vol. 30, pp. 280–284.

8. Zhang, Z., Frenzel, J., Neuking, K., and Eggeler, G., Vacuum induction melting of ternary NiTiX (X = Cu, Fe, Hf, Zr) shape memory alloys using graphite crucibles, *Mater. Trans.*, 2006, vol. 47, pp. 661–669.
9. Yang, S.Y., Kwon, Y., Choi, SW., et al., Diffusion pack cementation of hafnium powder with halide activator on Ni–Ti shape memory alloy, *J. Therm. Anal. Calorim.*, 2018, vol. 133, pp. 5–12.
10. Popov, N.N., Sysoeva, T.I., Aushev, A.A., Lar'kin, V.F., and Kostyleva, A.A., Properties of a 45Ti–45Ni–10Nb shape memory alloy in the as-cast and pressed states, *Russ. Metall.* (Engl. Transl.), 2016, vol. 2016, no. 11, pp. 1055–1063.
11. Kollerov, M.Yu., Ilyin, A.A., Pol'kin, I.S., Fainbron, A.S., Gusev, D.E., and Khachin, S.V., Structural aspects of the manufacture of semiproducts made from titanium nickelide-based alloys, *Russ. Metall.* (Engl. Transl.), 2007, vol. 2007, no. 5, pp. 408–414.
12. Kasimtsev, A.V., Markova, G.V., Shuitsev, A.V., Sviridova, T.A., and Volod'ko, S.S., Changes in the structure and properties of titanium hydride-calcium nickelide powder during rotational forging, *Tekhnol. Legk. Splavov*, 2016, no. 3, pp. 44–52.
13. Markova, G.V., Kasimtsev, A.V., Volod'ko, S.S., and Alimov, I.A., The effect of cross-helical rolling on the structure and properties of TiNi powder alloy: Part 2, *Tsvetn. Met.*, 2018, no. 12, pp. 75–81.
14. Kasimtsev, A.V. and Levinskii, Yu.V., *Gidridnokal'tsievye poroshki metallov, intermetallidov, tugoplavkikh soedinenii i kompozitsionnykh materialov* (Calcium Hydride Powders of Metals, Intermetallic Compounds, Refractory Compounds, and Composite Materials), Moscow: Mosk. Gos. Univ. Tonk. Khim. Tekhnol., 2012.
15. Kasimtsev, A.V., Volod'ko, S.S., Yudin, S.N., Sviridova, T.A., and Cheverikin, V.V., Synthesis of powder alloys based on the Ti–Ni–Hf system via a calcium hydride reduction process, *Inorg. Mater.*, 2019, vol. 55, no. 5, pp. 449–457.
16. Lyakishev, N.P., *Diagrammy sostoyaniya dvoinyh metallicheskih sistem* (State diagrams of binary metal systems), Moscow: Mashinostroenie, 1996, vol. 1.
17. Evirgen, A., Karaman, I., Santamarta, R., Pons, J., and Noebe, R.D., Microstructural characterization and shape memory characteristics of the $Ni_{50.3}Ti_{34.7}Hf_{15}$ shape memory alloy, *Acta Mater.*, 2015, vol. 83, pp. 48–60.
18. Umale, T., Salas, D., Tomes, B., Arroyave, R., and Karaman, I., The effects of wide range of compositional changes on the martensitic transformation characteristic of NiTiHf shape memory alloys, *Scr. Mater.*, 2019, vol. 161, pp. 78–83.

Translated by L. Mukhortova